SPACE-DELAY ADAPTIVE PROCESSING FOR MIMO RF INDOOR MOTION MAPPING

Chi Xu and Jeffrey Krolik

Department of Electrical and Computer Engineering, Duke University, Durham, NC 27708
chi.xu@duke.edu, jlk@duke.edu

ABSTRACT

In this paper, space-delay adaptive processing (SDAP) is proposed for motion mapping using MIMO RF signals. Typically, indoor RF localization methods require ultra-wideband signals to achieve the time-delay resolution required for separation of returns in complex multipath environments. Due to spectrum use restrictions, however, there is a need for methods which can operate using the lower bandwidths allocated for so-called ISM use. In this paper, we develop SDAP methods for linear MIMO transmit-receive arrays which can achieve near ultra-wideband range resolution and multipath sidelobe suppression but which use significantly less bandwidth. Real data results for indoor motion monitoring are presented aimed at mapping patient repositioning activities in long-term care facilities for pressure ulcer prevention.

Index Terms— MIMO, wide-area, motion monitoring, indoor multipath, bandwidth

1. INTRODUCTION

Wide-area RF-based indoor motion monitoring requires the ability to separate overlapping Doppler characteristics of multiple targets and analyze each target's motion based on its micro-Doppler signature. In [1], a sensor array transmitting wideband waveform was used to resolve the Doppler signature at a specific location by separately processing the fast-time samples and array wavefronts, known as ranging and beamforming. In [2], an ultra-wideband MIMO system was used for mitigating ghost motion returns due to indoor multipath scattering. However, conventional non-adaptive methods for ranging and beamforming degrade dramatically when signal bandwidth is more limited. Some range resolution improvement can be achieved by trading sidelobe level for mainlobe width, however, high sidelobe levels result in motion mapping artifacts which are easily confused with weaker targets in indoor environments.

While adaptive delay (i.e. fast-time samples) and spatial array processing can be applied sequentially to resolve slow-time sequences for micro-Doppler estimation from multiple targets, this separable processing is sub-optimal in multipath environments because of the complex coupling between signal time-delay and direction. In this paper, therefore, joint space-delay adaptive processing (SDAP) is presented. Furthermore, a reduced-rank solution for SDAP is derived, which is shown to outperform both non-adaptive and separate adaptive methods for real data.

1.1. Relation to Prior Work

The proposed method is related to space-time adaptive processing (STAP) [3], which jointly processes the slow-time samples and spatial array outputs to suppress non-separable clutter returns. Previous work for indoor motion monitoring used ultra-wideband signals to resolve and suppress multipath ambiguities [2, 4–6]. In this work, adaptive fast-time and spatial filtering are performed simultaneously to compensate for limited bandwidth. Slow-time samples of space-delay snapshots are used to estimate adaptive MIMO filter weights which permit discrimination of both direction-of-departure (DOD) and direction-of-arrival (DOA) for mitigating indoor multipath returns.

2. SPACE-DELAY SIGNAL MODEL

Consider a MIMO RF illuminator transmitting a sequence of M linear frequency modulated (LFM) chirps. Assume K transmit elements and N receive elements in the system. The waveform center frequency is f_c and bandwidth is B. Assuming L samples in each chirp, the returned signal is then a $L \times M \times N \times K$ hypercube. Let $x(l, m, n, k)$ denote signal at l-th fast-time sample, m-th pulse (slow-time sample), n-th receive element and k-th transmit element. In indoor environments, the total return is consisting of direct-path signals x_s, multipath returns x_p, clutter return x_c and noise x_ϵ,

$$x(l,m,n,k) = \sum_{i \in \mathcal{I}_s} x_s^i(l,m,n,k) \; + \sum_{i \in \mathcal{I}_p} x_p^i(l,m,n,k) \\ + \; x_c(l,m,n,k) \; + \; x_\epsilon(l,m,n,k) \qquad (1)$$

where $\mathcal{I}_s$ and $\mathcal{I}_p$ are index sets of direct-path and multipath returns, respectively. Let $\tau(m, n, k)$ denote the time-delay from k-th transmit element to a far-field point target and back to n-th receive element at m-th pulse. The returned signal after de-chirp processing is given by

$$z(l,m,n,k) \propto e^{-j2\pi \frac{BT_s l}{T_r} \tau(m,n,k)} e^{-j2\pi\left(f_c - \frac{B}{2}\right)\tau(m,n,k)} \qquad (2)$$

where T_r and T_s are the pulse repetition interval and sampling interval. The time-delay $\tau(m,n,k)$ is consisting of the group delay $\bar{\tau}(m)$ between the phase center of the transmit-receive arrays and the relative phase delay between transmit and receive elements $\tilde{\tau}(n,k)$. The phase delay can be further decomposed into receive array delay $\tilde{\tau}_r(n)$ and transmit array delay $\tilde{\tau}_t(k)$,

$$\begin{aligned}\tau(m,n,k) &= \bar{\tau}(m) + \tilde{\tau}(n,k) \\ &= \bar{\tau}(m) + \tilde{\tau}_r(n) + \tilde{\tau}_t(k)\end{aligned} \tag{3}$$

Assume a sufficiently narrowband waveform, the signal given in (2) can be rewritten in terms of $\bar{\tau}(m)$, $\tilde{\tau}_r(n)$ and $\tilde{\tau}_t(k)$ as

$$\begin{aligned}z(l,m,n,k) \;\propto\; & e^{-j2\pi\frac{B}{T_r}\tau_d T_s l}\; e^{-j2\pi f_c \bar{\tau}(m)} \\ & e^{-j2\pi f_c \tilde{\tau}_r(n)}\; e^{-j2\pi f_c \tilde{\tau}_t(k)}\end{aligned} \tag{4}$$

In (4), it is assumed that the group delay is much larger than the phase delay, and can be modeled as a constant in each coherent processing interval (CPI) for range processing, i.e. $\bar{\tau}(m) \approx \tau_d \gg \tilde{\tau}(n,k)$. This assumption is valid when the target is in the far-field and the waveform is sufficiently narrowband. The signal snapshot for SDAP is defined as

$$\begin{aligned}\mathbf{z}(m) = [\, & z(1,m,1,1) \;\; z(1,m,1,2) \;\; \cdots \;\; z(1,m,1,K) \\ \cdots \;\; & z(1,m,2,1) \;\; z(1,m,2,2) \;\; \cdots \;\; z(1,m,N,K) \;\; \cdots \\ & z(2,m,1,1) \;\; z(2,m,1,2) \;\; \cdots \;\; z(L,m,N,K)\,]^T\end{aligned} \tag{5}$$

The snapshot given in (5) is a $LNK \times 1$ vector, which is proportional to the Kronecker product of the fast-time vector $\mathbf{v}_d$, receive array vector $\mathbf{v}_r$ and transmit array vector $\mathbf{v}_t$,

$$\mathbf{z}(m) \;\propto\; e^{-j2\pi f_c \bar{\tau}(m)}\, \mathbf{v}_d(\tau_d) \otimes \mathbf{v}_r(\phi_r) \otimes \mathbf{v}_t(\phi_t) \tag{6}$$

The fast-time vector of return from a point target is a complex exponential with a frequency proportional to the delay τ_d,

$$\mathbf{v}_d(\tau_d) = \left[\, e^{-j2\pi\frac{B}{T_r}\tau_d T_s 1} \;\; \cdots \;\; e^{-j2\pi\frac{B}{T_r}\tau_d T_s L} \,\right]^T \tag{7}$$

If both the receive and transmit arrays are uniform linear arrays, the array vectors are complex exponentials with frequencies as functions of ϕ_r and ϕ_t,

$$\begin{aligned}\mathbf{v}_r(\phi_r) &= \left[\, e^{-j2\pi\frac{f_c}{c}d_r \sin\phi_r 1} \;\; \cdots \;\; e^{-j2\pi\frac{f_c}{c}d_r \sin\phi_r N} \,\right]^T \\ \mathbf{v}_t(\phi_t) &= \left[\, e^{-j2\pi\frac{f_c}{c}d_t \sin\phi_t 1} \;\; \cdots \;\; e^{-j2\pi\frac{f_c}{c}d_t \sin\phi_t K} \,\right]^T\end{aligned} \tag{8}$$

where ϕ_r and ϕ_t are the DOA and DOD of the signal, d_r and d_t are the inter-element spacing of the receive and transmit arrays. The model given in (1) can be rewritten in terms of SDAP snapshots as

$$\mathbf{x}(m) = \sum_{i\in\mathcal{I}_s} \mathbf{x}_s^i(m) + \sum_{i\in\mathcal{I}_p} \mathbf{x}_p^i(m) + \mathbf{x}_c(m) + \mathbf{x}_\epsilon(m) \tag{9}$$

The direct-path signal $\mathbf{x}_s(m)$ is the line-of-sight (LOS) return from point scatterers, which has identical DOD and DOA,

$$\mathbf{x}_s(m) = \alpha_s\, e^{-j2\pi f_c \bar{\tau}_s(m)}\, \mathbf{v}_d(\tau_s) \otimes \mathbf{v}_r(\phi) \otimes \mathbf{v}_t(\phi) \tag{10}$$

Different from direct-path signals, the multipath return $\mathbf{x}_p(m)$ can have arbitrary DOD and DOA,

$$\mathbf{x}_p(m) = \alpha_p\, e^{-j2\pi f_c \bar{\tau}_p(m)}\, \mathbf{v}_d(\tau_p) \otimes \mathbf{v}_r(\phi_r) \otimes \mathbf{v}_t(\phi_t) \tag{11}$$

For fixed transmit and receive systems, backscatter from walls and floors is at zero-Doppler thus can be removed by highpass filtering the slow-time sequence. With the clutter removed, the goal of motion mapping is to estimate the power in the slow-time sequence as a function of range (delay) and direction for LOS targets while mitigating ambiguities due to multipath scattering and space-delay filter sidelobes.

3. SPACE-DELAY ADAPTIVE PROCESSING

In this section, space-delay adaptive processing (SDAP) is discussed assuming the zero-Doppler clutter return has been removed by highpass filtering $\mathbf{x}(m)$ over m. After clutter removal, denote the clutter-free snapshot as $\mathbf{y}(m)$. The optimal SDAP filter weights are obtained by minimizing the expected power of filter outputs for interference, thus are given by

$$\mathbf{w}_{opt} = \mathbf{R}_u^{-1}\mathbf{v} \tag{12}$$

where $\mathbf{R}_u$ is the covariance matrix of non-target signal components and $\mathbf{v}$ is the target signal vector, which is the space-delay snapshot given in (5) at a specific delay and direction,

$$\mathbf{v} = \mathbf{v}_d(\tau) \otimes \mathbf{v}_r(\theta) \otimes \mathbf{v}_t(\theta) \tag{13}$$

For motion mapping, non-target signal components, i.e. interferences, include direct-path returns from other targets as well as multipath returns and noise. Since the measured data snapshot given in (9) contains direct-path and multipath returns from all locations, the "target-free" covariance matrix $\mathbf{R}_u$ is unavailable. Therefore, the data covariance matrix $\mathbf{R}_y$ is used and the minimum variance distortionless response (MVDR) weights are obtained by solving the constrained optimization problem [7],

$$\min_{\mathbf{w}}\; \mathbf{w}^H\mathbf{R}_y\mathbf{w} \qquad s.t.\; \mathbf{w}^H\mathbf{v} = 1 \tag{14}$$

and the solution is given by

$$\mathbf{w}_{mvdr} = \frac{\mathbf{R}_y^{-1}\mathbf{v}}{\mathbf{v}^H\mathbf{R}_y^{-1}\mathbf{v}} \tag{15}$$

3.1. A Reduced-Rank Solution

The optimal solution given in (15) requires the inverse of a covariance matrix with size $LNK \times LNK$. Moreover, a huge number of training snapshots are required to estimate the covariance matrix. In practice, reduced number of training snapshots, lower computation complexity and improved robustness of the adaptive filter can be achieved by reducing the degree of freedom (DOF) of the filter weights. In general, assume a low-rank weight vector solution given by

$$\mathbf{w}_{sol} = \mathbf{U}\mathbf{w}_{lr} \tag{16}$$

where $\mathbf{U}$ is a $LNK \times D$ matrix with orthonormal columns and $\mathbf{w}_{lr}$ is a $D \times 1$ weight vector. The optimization problem in (14) can be rewritten as

$$\min_{\mathbf{w}_{lr}} \mathbf{w}_{lr}^H \mathbf{U}^H \mathbf{R}_y \mathbf{U}\mathbf{w}_{lr} \quad s.t.\, \mathbf{w}_{lr}^H \mathbf{U}^H \mathbf{v} = 1 \tag{17}$$

and the low-rank MVDR solution is given by

$$\mathbf{w}_{sol} = \frac{\mathbf{U}\left(\mathbf{U}^H \mathbf{R}_y \mathbf{U}\right)^{-1} \mathbf{U}^H \mathbf{v}}{\mathbf{v}^H \mathbf{U}\left(\mathbf{U}^H \mathbf{R}_y \mathbf{U}\right)^{-1} \mathbf{U}^H \mathbf{v}} \tag{18}$$

The approach to choose $\mathbf{U}$ is an extension of beamspace beamforming [7]. Let $\mathbf{v}(\tau_0, \theta_0) = \mathbf{v}_d(\tau_0) \otimes \mathbf{v}_r(\theta_0) \otimes \mathbf{v}_t(\theta_0)$ denote the target signal vector at a particular delay τ_0 and direction θ_0. A few delays and directions around τ_0 and θ_0 are chosen, and the corresponding signal vectors are stacked to form a projection matrix $\mathbf{V}$ given by

$$\mathbf{V} = [\, \mathbf{v}(\tau_{-P}, \theta_{-P}) \ \cdots \ \mathbf{v}(\tau_P, \theta_{-P}) \ \cdots \ \mathbf{v}(\tau_P, \theta_P) \,] \tag{19}$$

Projecting data snapshot $\mathbf{y}(m)$ into the subspace spanned by $\mathbf{V}$ is essentially performing non-adaptive ranging and beamforming for a set of delays and directions around target location. Let $\mathbf{u}_1, \mathbf{u}_2, \cdots, \mathbf{u}_D$ denote the D singular vectors of $\mathbf{V}$ with largest singular values. The matrix $\mathbf{U}$ is obtained as

$$\mathbf{U} = [\, \mathbf{u}_1 \ \ \mathbf{u}_2 \ \ \cdots \ \ \mathbf{u}_D \,] \tag{20}$$

The choice of $\mathbf{V}$ projects the original high-dimensional data into a low-dimensional space while reserving most of the signal power. The choice of $\mathbf{U}$ further reduces the dimensionality and ensures orthonormality. Finally, the slow-time sequence at a specific delay τ and direction θ is given by

$$b_{\tau\theta}(m) = \mathbf{w}_{\tau\theta}^H \, \mathbf{y}(m) \tag{21}$$

where $\mathbf{w}_{\tau\theta}$ is obtained by (18), and $\mathbf{R}_y$ is estimated using the snapshots over slow-time pulses [8],

$$\widehat{\mathbf{R}}_y = \frac{1}{M} \sum_{m=1}^{M} \mathbf{y}(m)\mathbf{y}(m)^H \tag{22}$$

4. EXPERIMENTAL RESULTS

To evaluate the proposed method for wide-area indoor motion monitoring, real data experiments are conducted in the Michael W. Krzyzewski Human Performance Lab (K-Lab) at Duke University. The experimental set-up is shown in Fig. 1. The RF transmit-receive system in the foreground has 4 transmit elements and 16 receive elements, operating in the 2.4 GHz ISM band with a bandwidth of 150 MHz. The proposed method is developed for monitoring the motions of multiple long-term care patients in an indoor environment. In this experiment, the examining table in Fig. 1 was used as a surrogate patient bed which was shifted to different locations at which RF returns are measured. Measurements at multiple locations are summed to synthesize a multiple-target scenario. The main challenge of indoor motion monitoring is to detect motion locations in each CPI in the presence of multipath artifacts and sidelobes. This paper thus focuses on accurate motion mapping using limited bandwidth rather than classifying motions based on the micro-Doppler signature.

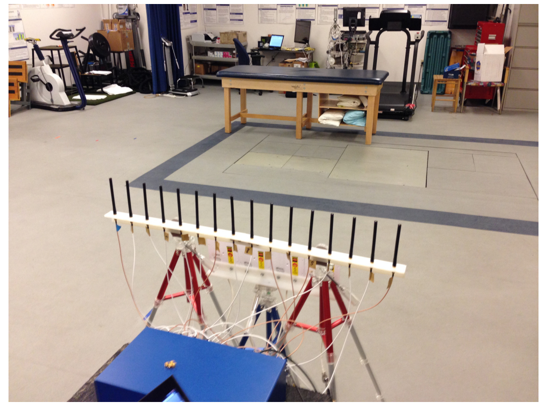

Fig. 1. MIMO RF illuminator and the lab scene.

To compare different processing methods, the power of the slow-time sequence given in (21) is plotted as a function of range and direction, which are shown in Fig. 2 to Fig. 6. For all maps, the truth is that there are two motions happening at 3 m and 5 m in range, respectively. Fig. 2 is the motion map obtained using ultra-wide bandwidth RF measurements, processed by conventional ranging and MIMO beamforming. The high-level sidelobes are not observable in the map since they are close to the mainlobe thus overlapped with the target. Fig. 3 to Fig. 6 are the motion maps obtained using 150 MHz bandwidth RF measurements. Fig. 2 is regarded as the ground truth for Fig. 3 to Fig. 6. It is shown in Fig. 3 that motion mapping ambiguities appear due to filter sidelobes. Hamming windowing is applied for suppressing the sidelobes and the corresponding motion map is shown in Fig. 4. Although sidelobe levels are suppressed, the enlarged mainlobe degrades the resolution and creates mapping ambiguities due to the fixed filter response pattern.

Fig. 5 shows the motion map obtained by applying adaptive ranging and adaptive beamforming separately. This method successfully mitigates the sidelobe ambiguities. However, the separate adaptive filter designs a filter response pattern that is separable in range and direction, thus is sub-

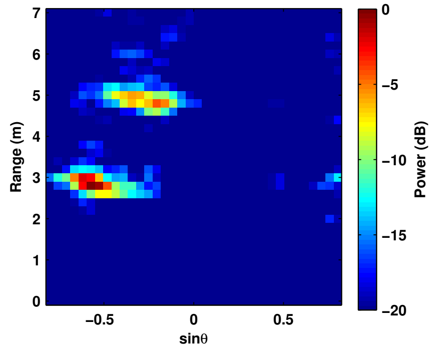

Fig. 2. Non-adaptive processing, 600 MHz bandwidth.

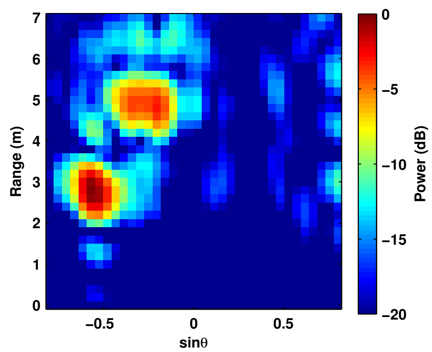

Fig. 3. Non-adaptive processing, 150 MHz bandwidth.

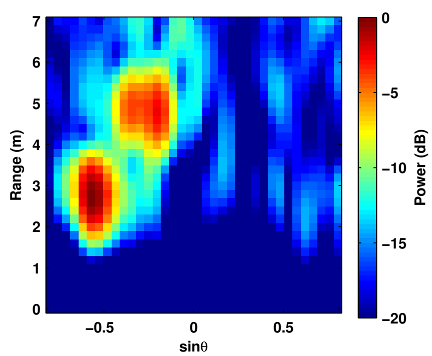

Fig. 4. Hamming window processing, 150 MHz bandwidth.

optimal for suppressing non-separable returns. In indoor environments, moving targets generate direct-path returns as well as multipath returns due to local scattering. Unlike point targets, the real target return typically spreads in range and direction. As a result, the separate filter squeezes its mainlobe to suppress interferences which are closely located to the target location, thus amplifying the background noise at other locations. In contrast, the SDAP filter operates in a high-dimensional space where the returns from different targets are well-separated thus can be suppressed using a few

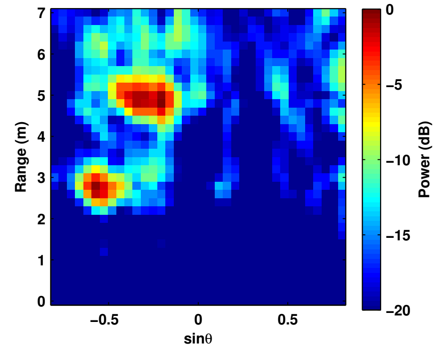

Fig. 5. Separate adaptive processing, 150 MHz bandwidth.

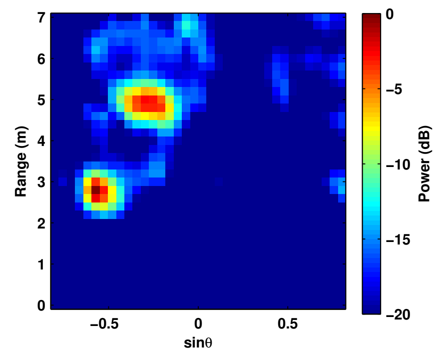

Fig. 6. Joint adaptive processing, 150 MHz bandwidth.

DOF. The motion map obtained using SDAP is shown in Fig. 6, which outperforms the non-adaptive and separate adaptive methods.

5. CONCLUSION AND FUTURE WORK

In this paper, fast-time samples and spatial array outputs are jointly processed to resolve the slow-time sequence at LOS locations in a wide-area indoor multipath environment. The proposed method successfully mitigates mapping ambiguities due to multipath and sidelobes with limited signal bandwidth. Although the 150 MHz bandwidth used here is wider than the 2.4 GHz ISM band, it matches the ISM band from 5.725 to 5.875 GHz. Future work includes developing indoor motion monitoring methods using distributed RF sensors.

6. ACKNOWLEDGMENT

This work is supported by the Information Initiative at Duke (i.i.D.). The authors would also like to thank Dr. Robin Queen of the Duke K-Lab for collecting real data, and collaboration with Dr. Tracey Yap and Dr. Kirsten Corazzini of the Duke School of Nursing on this project.

7. REFERENCES

[1] S. S. Ram, Y. Li, A. Lin, and H. Ling, "Doppler-based detection and tracking of humans in indoor environments," *Journal of the Franklin Institute*, vol. 345, no. 6, pp. 679–699, 2008.

[2] C. Xu and J. Krolik, "MIMO RF probe for wide-area indoor human motion monitoring," in *Acoustics, Speech and Signal Processing (ICASSP), 2014 IEEE International Conference on*. IEEE, 2014, pp. 6047–6051.

[3] J. Ward, "Space-time adaptive processing for airborne radar," 1998.

[4] X. P. Masbernat, M. G. Amin, F. Ahmad, and C. Ioana, "An MIMO-MTI approach for through-the-wall radar imaging applications," in *Waveform Diversity and Design Conference (WDD), 2010 International*. IEEE, 2010, pp. 188–192.

[5] A. Martone, K. Ranney, and R. Innocenti, "Automatic through the wall detection of moving targets using low-frequency ultra-wideband radar," in *Radar Conference, 2010 IEEE*. IEEE, 2010, pp. 39–43.

[6] T. S. Ralston, G. L. Charvat, and J. E. Peabody, "Real-time through-wall imaging using an ultrawideband multiple-input multiple-output (MIMO) phased array radar system," in *Phased Array Systems and Technology (ARRAY), 2010 IEEE International Symposium on*. IEEE, 2010, pp. 551–558.

[7] H. L Van Trees, *Detection, estimation, and modulation theory, optimum array processing*, John Wiley & Sons, 2004.

[8] J. Yu and J. Krolik, "MIMO adaptive beamforming for nonseparable multipath clutter mitigation," *Aerospace and Electronic Systems, IEEE Transactions on*, vol. 50, no. 4, pp. 2604–2618, 2014.